ACS APPLIED MATERIALS & INTERFACES

Research Article

www.acsami.org

Direct Low-Temperature Growth of Single-Crystalline Anatase TiO_2 Nanorod Arrays on Transparent Conducting Oxide Substrates for Use in PbS Quantum-Dot Solar Cells

Hyun Suk Chung,[†,⊥] Gill Sang Han,[†,⊥,▽] So Yeon Park,[†] Hee-Won Shin,[‡] Tae Kyu Ahn,[‡] Sohee Jeong,[§,#] In Sun Cho,*[,∥] and Hyun Suk Jung*[,†]

[†]School of Advanced Materials Science & Engineering and [‡]Department of Energy Science, Sungkyunkwan University, Suwon 440-746, Korea

[§]Nanomechanical Systems Research Division, Korea Institute of Machinery and Materials (KIMM), Daejeon 305-343, Korea

[∥]Department of Materials Science and Engineering & Energy Systems Research, Ajou University, Suwon 443-749, Korea

[#]Department of Nanomechatronics, Korea University of Science and Technology (UST), Daejeon 305-350, Korea

[▽]Department of Mechanical Engineering and Materials Science, University of Pittsburgh, Pittsburgh, Pennsylvania 15261, United States

Supporting Information

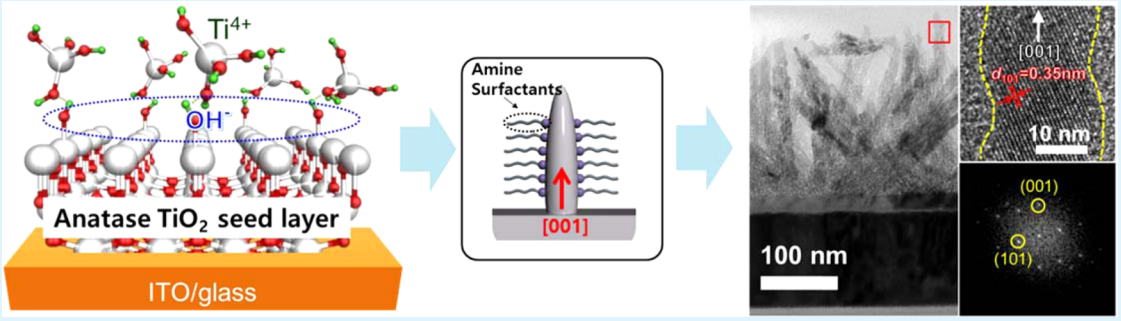

ABSTRACT: We report on the direct growth of anatase TiO_2 nanorod arrays (A-NRs) on transparent conducting oxide (TCO) substrates that can be directly applied to various photovoltaic devices via a seed layer mediated epitaxial growth using a facile low-temperature hydrothermal method. We found that the crystallinity of the seed layer and the addition of an amine functional group play crucial roles in the A-NR growth process. The A-NRs exhibit a pure anatase phase with a high crystallinity and preferred growth orientation in the [001] direction. Importantly, for depleted heterojunction solar cells (TiO_2/PbS), the A-NRs improve both electron transport and injection properties, thereby largely increasing the short-circuit current density and doubling their efficiency compared to TiO_2 nanoparticle-based solar cells.

KEYWORDS: *anatase TiO_2, nanorod arrays, low-temperature solution growth, depleted heterojunction solar cells, charge transport*

INTRODUCTION

Lead sulfide (PbS) quantum dots (QDs) have shown high potential for low-cost, large-area, and high-efficiency photovoltaic devices, given their large Bohr radius, size-dependent tunable band gap across the near-infrared (near-IR) region, and large absorption cross-section.[1−4] In addition, solution processing in ambient conditions using colloidal QDs (CQDs) offers a facile and large-scale preparation method for photovoltaic devices.[5−7]

In the past few years, Schottky-type PbS QD solar cells have drawn significant interest because of their simple device structure.[8,9] However, some drawbacks, such as a low built-in voltage caused by a low work function of the metal electrode and the large recombination produced by leakage of holes through the junction, limit their device performance.[10] A new device architecture, depleted heterojunction (DH) solar cells, which is of current interest, can solve these drawbacks. DH solar cells are based on a heterojunction between the PbS QDs and oxide semiconductors (such as TiO_2 and ZnO), in which the large band gap of the oxide semiconductor enables a hole blocking mechanism, allowing the use of metal electrodes with low work functions.[10−13] Despite these advantages, DH solar cells still exhibit a limited performance compared to other thin film photovoltaic devices, which is associated with various trap phenomena in the PbS QDs.[14] In addition, absorption of light and charge extraction (i.e., smaller diffusion length of ∼10 nm and depletion layer width) characteristics still limits the performance improvement.

Received: February 3, 2015
Accepted: April 30, 2015
Published: April 30, 2015

DOI: 10.1021/acsami.5b00948
ACS Appl. Mater. Interfaces 2015, 7, 10324−10330

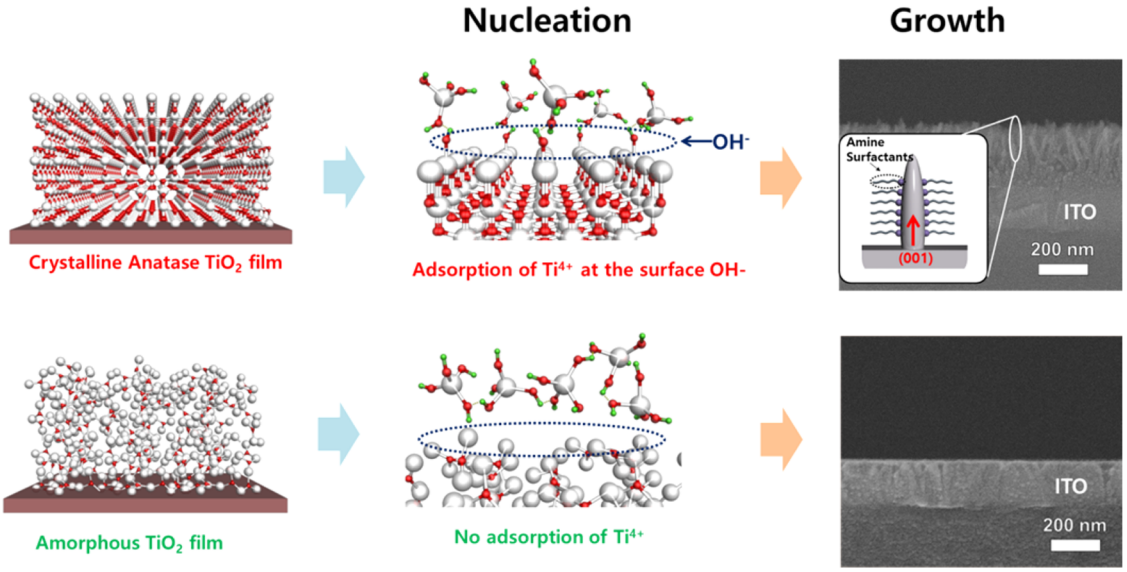

Figure 1. Schematic of the growth mechanism of anatase TiO_2 nanorods (A-NRs). A crystalline seed layer and the selective adsorption of an amine group are the key factors to ensure the direct growth of A-NRs on Sn-doped In_2O_3 (ITO)/glass substrates.

One feasible approach to resolve these issues is to control the device architecture by introducing a nanostructured oxide semiconductor. Especially, single-crystalline TiO_2 nanorods/nanowires grown directly on transparent conducting oxide (TCO) electrodes provide a perfect solution to avoid particle-to-particle hopping that occurs in polycrystalline films, thereby increasing the photocurrent efficiency. In addition to their potential for electron transport improvement, they also enhance light harvesting by scattering of the incident light. For instance, Gonfa et al. and Li et al. studied rutile TiO_2 nanorod-based DH solar cells, in which one-dimensional (1D) TiO_2 nanorods enabled a fast charge collection, thus demonstrating improved solar cell efficiencies.[15−18] Kamat et al. reported that TiO_2 nanotubes decorated with CdSe quantum dots facilitate charge transport and light harvesting processes.[19] Aydil et al. also demonstrated a single-crystalline TiO_2 nanrods/nanoflakes array improves dye-sensitized solar cell performance.[20] All of these reports showed the effectiveness of nanostructure engineering in order to improve the solar cell efficiency through synthesis of TiO_2 nanorods/pillars. However, most of the proposed approaches are based on rutile TiO_2 rather than anatase TiO_2, the latter being more favorable when it comes to photovoltaic performance.[21−23]

Here, we report on the direct growth of anatase TiO_2 nanorod arrays on tin-doped indium oxide/glass (ITO) substrates by a simple hydrothermal method. Our method is based on a local epitaxial growth and conducted in a mild hydrothermal condition (140 °C, pH ∼ 10), hence minimizing the FTO/glass damage and enabling intimate contact with ITO/glass substrate (Supporting Information Table S1). Critical experimental parameters that affect the growth of anatase TiO_2 nanorods (A-NRs) are investigated, and detailed crystallographic characteristics of the synthesized TiO_2 nanorods are also examined. Importantly, we showed that the A-NRs improve the charge transport and collection efficiencies for DH solar cells (TiO_2/PbS) via the increase of the photocurrent generation, and thus doubling the solar cell efficiency.

EXPERIMENTAL SECTION

Growth of Anatase TiO_2 NRs on ITO or FTO Substrates. A-NRs were grown directly on tin-doped In_2O_3 (ITO) or fluorine-doped SnO_2 substrates by previously reported hydrothermal method with further modification.[24,25] First, a TiO_2 thin film seed layer was deposited on cleaned ITO/glass substrates by atomic layer deposition (ALD), followed by thermal annealing at 450 °C for 1 h. Second, a stock solution for NR growth was prepared by mixing 0.4 M titanium tetraisopropoxide (TTIP; 97%; Sigma-Aldrich), 0.4 M triethanolamine (TEOA; 99%; Sigma-Aldrich), and 0.4 M ethylendiamine (99%; Sigma-Aldrich) in deionized (DI) water. The ITO/glass substrates coated with the seed layers were immersed in the stock solution and then placed in an electric oven (90 °C for 24 h) for the gelation reaction. After this process, the oven was heated to 140 °C to grow TiO_2 NRs (48 h). The resultant TiO_2 NRs were washed with DI water several times and finally annealed at 450 °C for 1 h in air. For comparison, anatase TiO_2 nanoparticles were synthesized using a similar method.[25]

Synthesis of the PbS Colloidal QD Solution. The PbS QDs were synthesized via the hot-injection method.[26] A lead oleate solution was prepared for the reaction solution; 0.002 M lead(II) oxide powder (PbO; 99%; Sigma-Aldrich) and 0.004 M oleic acid (90%; Sigma-Aldrich) were dissolved in octadecene (90%; Sigma-Aldrich). The prepared reaction solution was heated to 100 °C in a three-neck flask. After the lead oxide was completely decomposed to form lead oleate (indicated by a color change of the solution from yellow to clear/transparent), the temperature of the solution was raised to 120 °C. Then, an injection solution, which consisted of 0.001 M hexamethyldisilathiane (synthesis grade; Sigma-Aldrich) in octadecene, was rapidly injected into the lead oleate solution in order to synthesize the PbS QDs. After the reaction, PbS QDs were washed several times using toluene and finally dispersed in an octane solution (10 mg/mL).

Fabrication of Solar Cells. PbS/TiO_2 solar cells were fabricated by spin-coating the PbS QD solution layer-by-layer on the TiO_2 nanorod array.[11] Each layer was spin-coated by dispensing 200 μL of the QD solution on a 2 × 2 cm^2 substrate using a rotation velocity of 2500 rpm for 10 s. To cross-link the QDs, 10% mercaptopropionic acid (99%; Sigma-Aldrich) in a methanol solution was spin-coated, after which octane was spin-coated on the substrates to rinse the remaining QDs. For the top electrode, an Ag film (50 nm) was coated via thermal evaporation.

Characterizations. The TiO_2 NR structures and solar cell architectures were observed by field-emission scanning electron

DOI: 10.1021/acsami.5b00948
ACS Appl. Mater. Interfaces 2015, 7, 10324−10330

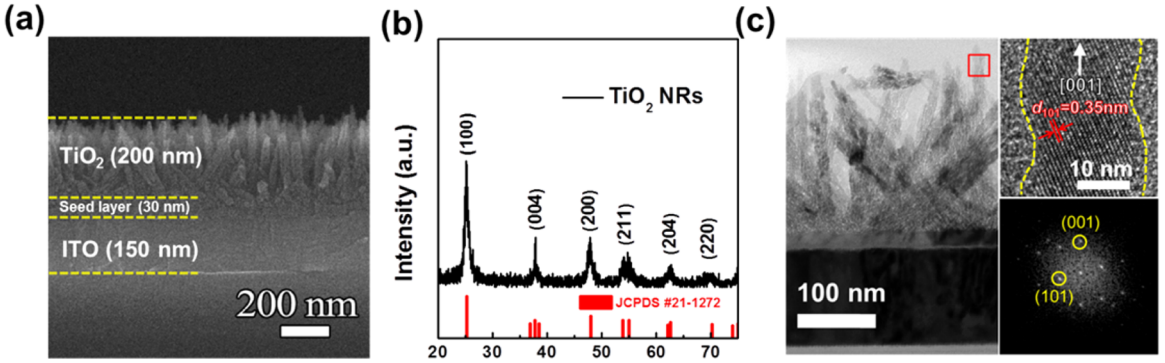

Figure 2. Structural properties of the anatase TiO_2 nanorods (A-NRs): (a) Cross-sectional SEM image of A-NRs on an ITO/glass substrate, (b) a typical XRD pattern, and (c) cross-sectional TEM image and the corresponding HR-TEM image and its FFT pattern, showing that the A-NRs grow in the [001] direction with exposed {101} surface facets on the sides.

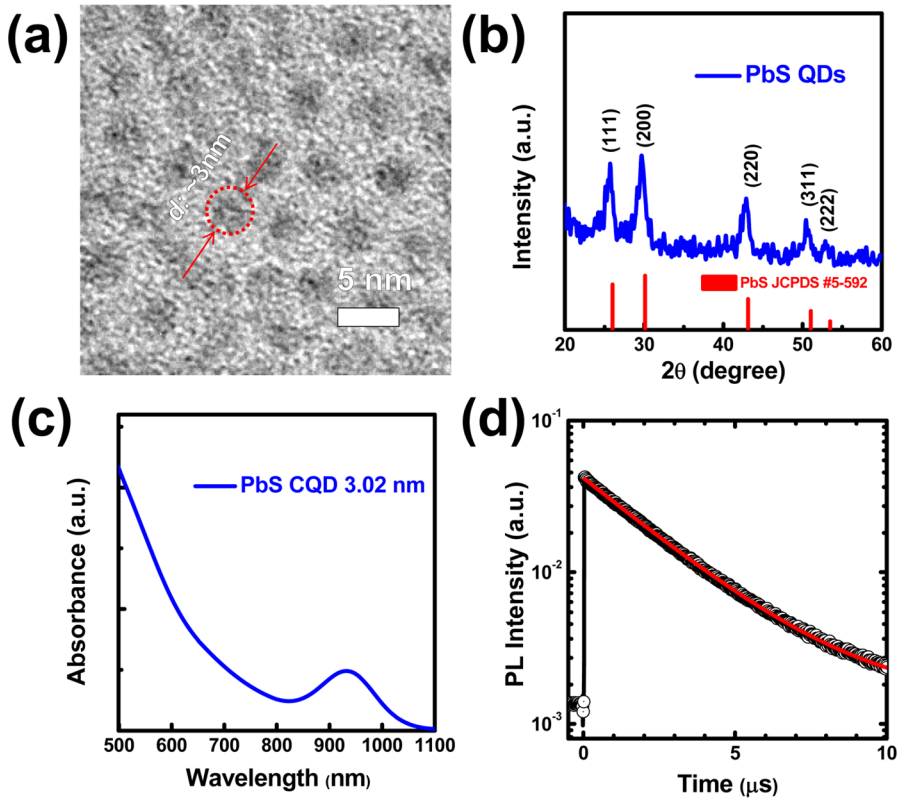

Figure 3. Structural and optical properties of synthesized PbS quantum dots (QDs): (a) TEM image, (b) XRD pattern, and (c) absorption spectrum of the synthesized PbS QDs used in the device fabrication. (d) Transient photoluminescence emission decays for a wavelength of 1000 nm. Solid red lines: fits to single-exponential decay functions.

microscopy (FE-SEM; JSM-7600F, JEOL). The material morphology and crystallinity were identified using high-resolution transmission electron microscopy (HR-TEM; JEM-3010, JEOL) and X-ray diffraction (XRD; D8 discover, Bruker), respectively. The optical properties of the QDs were measured by UV/vis spectrometry (PerkinElmer). Photovoltaic properties were measured by a potentiostat (CHI660, CHI Instrument) under air mass (AM) 1.5 simulated solar light illuminations (Oriel Sol 3A class AAA, Newport). The transient photoluminescence emission decay was observed with an near-IR laser system. In these systems, the emissions were triggered by Nd:YAG pulsed lasers (Quanta Ray Pro, Spectra-Physics) through an ND filter, while the emission decays were detected by a photomultiplier tube module (H10330-75, Hamamatsu Photonics) equipped with a monochromator (Acton SP 2300, Princeton Instruments).

RESULTS AND DISCUSSION

A-NRs were directly grown on ITO/glass substrates using a two-step hydrothermal method.[24,25] A schematic description of their growth mechanism is shown in Figure 1. A TiO_2 thin film (30 nm in thickness), which acts as a seed layer, was first deposited by atomic layer deposition (ALD), followed by a thermal annealing to ensure crystallization. For comparative purposes, amorphous TiO_2 thin films were also deposited by ALD without being subjected to the subsequent thermal annealing. A micro-Raman analysis confirmed that the thermally annealed TiO_2 film has an anatase phase, while the film without the post-thermal annealing exhibits an amorphous phase (Supporting Information Figure S1) We found that, during the growth process, the crystallinity of the TiO_2 thin

DOI: 10.1021/acsami.5b00948
ACS Appl. Mater. Interfaces 2015, 7, 10324−10330

film plays a critical role when it comes to the growth of 1D A-NRs, since the anatase seed layer affects the gelation process. According to the X-ray photoelectron spectroscopy (XPS) analysis (Supporting Information Figure S2), the annealed seed layer (anatase phase) has more surface hydroxyl (OH^-) groups than the nonannealed seed layer (amorphous), reflecting that the anatase seed layer offers more adsorption sites for Ti^{4+} hydroxylation to form $Ti(OH)_4$. In the second growth step, the nucleation and growth occurred at a higher temperature (140 °C). In this step, the amine groups are selectively adsorbed onto the {101} and {100} surfaces, hence enabling the anisotropic growth of TiO_2 in the [001] direction,[18,21] leaving exposed {101} and {100} facets on the side. On the other hand, no growth was observed for the nonannealed seed layer, because of the insufficient amount of surface OH^- groups, thereby impeding the nucleation process.[24]

Figure 2a shows a cross-sectional SEM image of the A-NRs grown on the ITO/glass substrate. The A-NRs have an average length of 200 nm and a diameter of ~50 nm. The XRD pattern (Figure 2b) clearly shows that all diffraction peaks of the A-NRs match the tetragonal anatase TiO_2 phase (JCPDS No. 21-1272); i.e., the TiO_2 NRs grown on the ITO/glass substrate possess a pure anatase phase. Importantly, the relative intensity of the (004) peak is obviously higher compared to the standard reference peak, suggesting the A-NRs have a preferred growth orientation of the [001] direction (Supporting Information Figure S3). In order to further check the crystallographic features (growth direction, size, and crystallinity), a cross-sectional TEM analysis was conducted after a focused-ion-beam (FIB) milling. As shown in Figure 2c, the A-NRs have a narrow size distribution (an average diameter of ~50 nm) and show a high crystallinity with a tetragonal anatase phase. Additionally, the HR-TEM image and fast Fourier transform (FFT) pattern confirm that A-NRs grow along the [001] direction and have a rough surface with exposed surface facets of the {101} planes.

The A-NRs were further compared with rutile TiO_2 nanorods arrays (R-NRs, thickness = 200 nm and diameter = ~60 nm) that were prepared by a previously reported hydrothermal method (170 °C/(90 min)).[27] As shown in Supporting Information Figure S4, although the A-NRs have less light absorption (due to their larger band gap, ~3.2 eV), they show higher flat band potential (i.e., higher conduction band edge position), lower bulk recombination resistance, and better surface catalytic activity than the R-NRs with similar morphology.

Next, the PbS CQDs that were used for the fabrication of DH solar cells were synthesized via the previously reported hot-injection method with further modifications.[26] Figure 3a shows a TEM image of the synthesized PbS QDs. The PbS QDs have an average size of 3.0 ± 0.1 nm with a narrow size distribution. The XRD pattern of the PbS QDs shows that all diffraction peaks match with the tetragonal PbS phase as shown in Figure 3b (JCPDS No. 5-592). Figure 3c shows the absorbance of the PbS QD solution dispersed in octane. First, the shoulder peak around 920 nm has a narrow width (i.e., a small full width at half-maximum), indicating that the synthesized QDs have a narrow size distribution as confirmed by the previous TEM image. An experimental relationship between the average QD size (d) and the band gap ($E_{bandgap}$) is expressed by eq 1. The QD band gap is correlated to the wavelength (λ) at which the maximum of absorbance peak occurs (eq 2),[28] where d is the average QD size, h is Plank's constant (4.135×10^{-15} eV·s), and c is the speed of light (2.998×10^8 m/s).

$$E_{bandgap} = 0.41 + (0.025d^2 + 0.283d)^{-1} \quad (1)$$

$$E_{bandgap} = \frac{hc}{\lambda} \quad (2)$$

According to the preceding equations, the maximum absorbance peak at 920 nm results in an average QD size of 3.0 nm, which agrees well with the results from the TEM analysis. The PbS QDs with different sizes were also synthesized by controlling the reaction temperature (Supporting Information Figure S5). The transient photoluminescence emission decay of the PbS QDs is shown in Figure 3d. The detector records the emission at an IR wavelength of 1000 nm. These data can be fitted to the exponential decay function shown in eq 3,[29] where A and C are constants, t is time (μs), and τ is the emission decay lifetime constant.

$$I_{PL}(t) = C + A \exp\left(-\frac{t}{\tau}\right) \quad (3)$$

The red line in Figure 3d represents the fitting curve according to the function in eq 3. The obtained value for τ was 2.64 μs, which, although being somewhat large, is consistent with previous reports of same-sized QDs, ensuring sufficient time for hole transport to take place.[30]

Using the previously mentioned A-NRs (200 nm in length) and PbS QDs (3.0 nm in size), we fabricated DH PbS QD solar cells. For comparative purposes, DH solar cells based on TiO_2 nanoparticles (NPs) with an average size of 20 nm were also prepared. Based on previous studies, PbS QDs with a size of 3.0 nm were selected since they have a higher charge transfer efficiency to TiO_2.[31] Figure 4a shows cross-sectional SEM images of A-NRs and NP-based DH solar cells. To ensure a fair comparison, the thickness of the TiO_2 layer was fixed to 200 nm and PbS QDs layers with the same thickness were deposited on top of the TiO_2 layer. As a top electrode, a Ag film with a thickness of 50 nm was finally deposited by e-beam evaporation. As shown in the figure, the PbS QDs are fully infiltrated into the TiO_2 layer without showing any voids in both DH solar cells.

Figure 4b shows representative $J-V$ curves for both DH solar cells measured under AM 1.5G simulated solar light illumination (100 mW/cm^2), and the corresponding photovoltaic parameters are listed in Table 1. Interestingly, the DH solar cell based on A-NRs exhibited a much higher photovoltaic performance than the DH solar cell based on TiO_2 NPs. In particular, the short-circuit current density (J_{sc}) for the A-NRs was 1.6 times higher than that of the TiO_2 NPs, implying a more efficient charge collection for the former structures, i.e., higher transport and transfer properties (this will be discussed later). Additionally, the A-NR DH solar cell shows a higher fill factor (FF; ~16%) than its NP-based counterpart. On the other hand, the open-circuit voltage (V_{oc}) values were similar for both DH solar cells. As a result, the A-NRs-based DH solar cell exhibited a solar cell efficiency approximately two times higher (1.6% for A-NRs and 0.9% for TiO_2 NPs) than that for the anatase NP-based DH solar cell, demonstrating the effective use of A-NRs for PbS solar cell applications.

In order to understand the improved performance of the A-NR DH solar cell, the bulk recombination properties were examined by measuring the transient V_{oc} decay and photoluminescence (PL) emission decay curves.[29,32] Figure 5a shows the charge carrier lifetime curves of both the A-NRs and A-NPs DH solar cells, which were obtained from the transient V_{oc}

DOI: 10.1021/acsami.5b00948
ACS Appl. Mater. Interfaces 2015, 7, 10324−10330

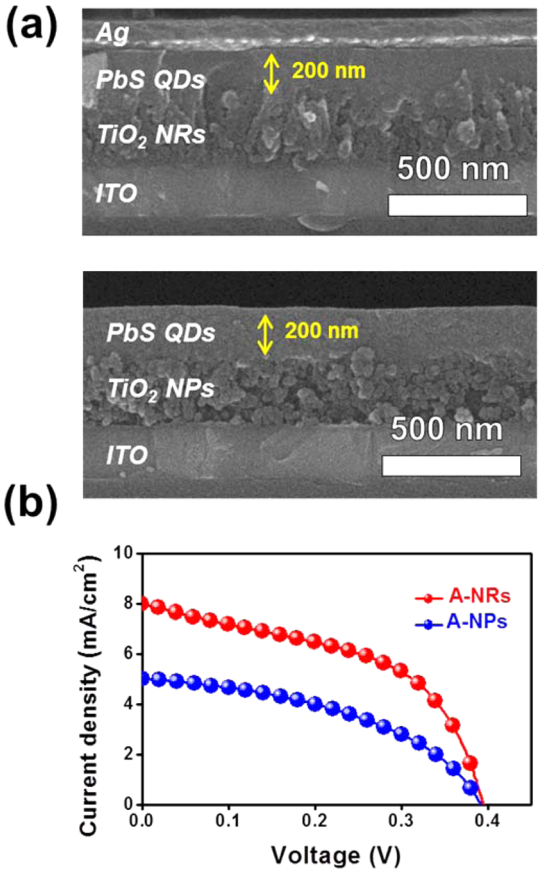

Figure 4. Fabricated depleted heterojunction (DH) solar cells using anatase TiO_2 nanorods (A-NRs) and nanoparticles (NPs): (a) Cross-sectional SEM images of TiO_2 NR- and NP-based DH solar cells at the top and bottom, respectively, and (b) the corresponding $J-V$ curves showing that the use of A-NRs assures a 1.6 times higher photocurrent density.

Table 1. Summary of the Solar Cell Parameters Corresponding to DH Solar Cells Based on Either Anatase TiO_2 Nanorods (NRs) or Nanoparticles (NPs)[a]

TiO_2 morphology	J_{sc} (mA/cm^2)	V_{oc} (V)	FF (%)	PCE (%)
TiO_2 NRs	8.3 ± 2.0	0.41 ± 0.03	51 ± 5	1.6 ± 0.3
TiO_2 NPs	5.2 ± 2.3	0.39 ± 0.04	44 ± 5	0.9 ± 0.2

[a]In order to calculate the standard deviation, at least three devices of the type of solar cell were fabricated and characterized.

decay analysis (Supporting Information Figure S6). Throughout the entire potential range, a much higher charge carrier lifetime was found for the A-NR DH solar cell than for the A-NP-based DH solar cell, suggesting that the A-NRs induce less recombination, hence showing improved charge transport properties. In general, single-crystalline nanorods/nanowires exhibit improved charge transport properties for solar cell applications since they provide direct transport channels for electrons and holes to the electrodes and feature higher electron mobility. Moreover, for DH solar cells (similar to p–n junction solar cells), the smaller junction area in NR-based solar cells when compared to NP-based ones is advantageous in order to reduce the junction recombination.[33] As a result, these two features in A-NR-based DH solar cells ensure improved charge transport efficiency. Furthermore, transient PL emission decay curves of PbS/TiO_2 junction devices are shown in Figure

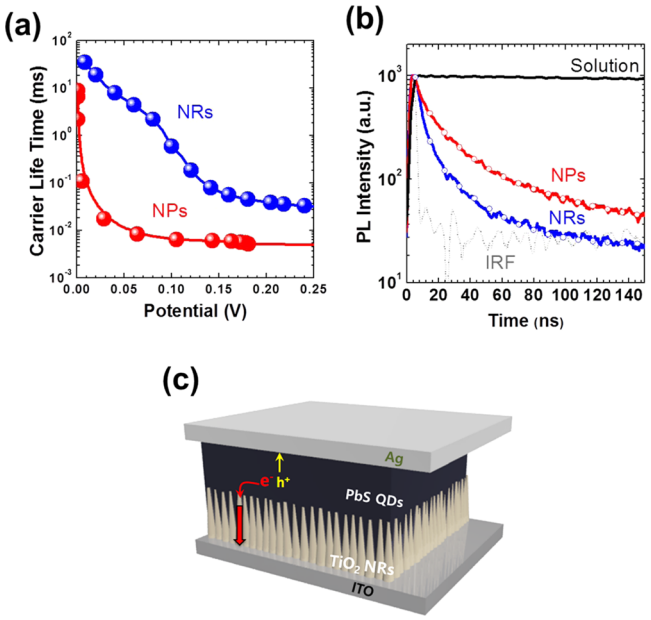

Figure 5. Characterization of charge carrier lifetime and injection properties of anatase TiO_2 nanorod (A-NR)- and A-NP-based DH solar cells: (a) Carrier lifetime estimated from the transient open-circuit voltage (V_{oc}) decay, (b) transient photoluminescence emission decay curves of PbS/TiO_2 junction devices, and (c) schematic of a TiO_2 NR/PbS QD junction illustrating less bulk recombination of charge carriers due to fast electron injection and transport.

5b. Interestingly, the PbS/TiO_2 junction device based on NRs shows a much faster decay than the device based on NPs, implying a much faster electron injection.[29] To compare the time constants quantitatively, the PL emission data were fitted to a triple exponential decay function (eq 4),[29] where $I_{PL}(t)$ is photoluminescence intensity, C is constant, A_n is the characteristic exponential amplitude, and t is time, and a mean emission decay lifetime (τ_{mean}) was obtained with eq 5.

$$I_{PL}(t) = C + A_1 \exp\left(-\frac{t}{\tau_1}\right) + A_3 \exp\left(-\frac{t}{\tau_2}\right) + A_3 \exp\left(-\frac{t}{\tau_3}\right) \quad (4)$$

$$\tau_{mean} = \frac{\sum_{n=1}^{3} A_n \tau_n^2}{\sum_{n=1}^{3} A_n \tau_n} \quad (5)$$

The obtained time constant values are listed in Supporting Information Table S2. The A-NR/PbS junction device exhibits much smaller time constants than the A-NPs/PbS junction device. Especially, regarding τ_{mean}, the A-NRs/PbS device exhibits a value of 11.05 ns and hence is three times faster than the A-NPs/PbS device, thus, reflecting a much faster electron injection for the former device type.

The distinct features of single-crystalline A-NRs for DH solar cells are schematically summarized in Figure 5c. First, the single-crystalline 1D nature of the A-NRs reduces bulk recombination by fast electron transport. Second, the unique surface structure of A-NRs (see the TEM analysis in Figure 1c) enables an intimate contact between TiO_2 and PbS, thereby possibly retarding the interface (junction) recombination through fast electron injection into TiO_2. Therefore, these two features, enable a higher J_{sc} and FF in A-NR-based solar cells when compared to the DH solar cells based on A-NPs.

DOI: 10.1021/acsami.5b00948
ACS Appl. Mater. Interfaces 2015, 7, 10324–10330

CONCLUSIONS

In summary, we have grown single-crystalline A-NRs on ITO substrates via a seed layer mediated epitaxial growth using a two-step hydrothermal method. We found that the crystallinity of the seed layer plays a crucial role in the growth process, i.e., the adsorption/hydroxylation of Ti^{4+} ions. Additionally, absorption of an amine group during the nucleation and growth processes facilitates the anisotropic growth of A-NRs. The resultant TiO_2 NRs have a high crystallinity and exhibit preferred growth in the [001] direction with exposed {101} facets. When combined with PbS QDs, in order to create DH solar cells, the NRs show improved electron transport and injection properties, which increase their short-circuit current density, thereby doubling the TiO_2/PbS DH solar cell efficiency. We believe that the efficiency of A-NR-based DH solar cells will increase further with additional optimization of the A-NR morphology and PbS deposition process. Besides, we also consider that A-NRs will impact other types of solid-state solar cells that require TiO_2 as an electron transport layer such as perovskite solar cells.

ASSOCIATED CONTENT

Supporting Information

Tables listing comparison of anatase TiO_2 nanorods/nanowires growth methods and a summary of the photoluminescence emission decay lifetime constants of PbS/TiO_2 junction devices and figures showing Raman and XPS spectra of ALD-deposited TiO_2 films, XRD patterns of the anatase TiO_2 nanorods array and nanoparticle film, a texture coefficient plot, plots comparing morphology, light absorption, electrochemical properties, and charge tranfer efficiencies between anatase and rutile TiO_2 nanorod arrays, absorption spectra of synthesized PbS quantum dots, and V_{oc} decay curves of DH solar cells. The Supporting Information is available free of charge on the ACS Publications website at DOI: 10.1021/acsami.5b00948.

AUTHOR INFORMATION

Corresponding Authors

*(I.S.C.) Tel.: +82-31-219-2468. Fax: +82-31-219-1613. E-mail: insuncho@ajou.ac.kr.

*(H.S.J.) Tel.: +82-31-290-7403. Fax: +82-31-290-7410. E-mail: hsjung1@skku.edu.

Author Contributions

⊥H.S.C. and G.S.H. contributed equally to this work.

Notes

The authors declare no competing financial interest.

ACKNOWLEDGMENTS

This work was supported by the National Research Foundation of Korea (NRF) grants funded by the Ministry of Science, ICT & Future Planning (MSIP) of Korea under Contract Nos. NRF-2014R1A4A1008474, 2014R1A2A2A01007722, 2012M3A7B4049967(Nano.Material Technology Development Program), and 2012M3A6A7054861 (Global Frontier R&D Program on Center for Multiscale Energy System).

REFERENCES

(1) Nozik, A. J. Quantum dot solar cells. *Phys. E* **2002**, *14*, 115−120.

(2) Ellingson, R. J.; Beard, M. C.; Johnson, J. C.; Yu, P.; Micic, O. I.; Nozik, A. J.; Shabaev, A.; Efros, A. L. Highly Efficient Multiple Exciton Generation in Colloidal PbSe and PbS Quantum Dots. *Nano Lett.* **2005**, *5*, 865−871.

(3) Klimov, V. I. *Nanocrystal quantum dots*; CRC Press: Boca Raton, FL, USA, 2010.

(4) McDonald, S. A.; Konstantatos, G.; Zhang, S.; Cyr, P. W.; Klem, E. J. D.; Levina, L.; Sargent, E. H. Solution-processed PbS quantum dot infrared photodetectors and photovoltaics. *Nat. Mater.* **2005**, *4*, 138−142.

(5) Gur, I.; Fromer, N. A.; Geier, M. L.; Alivisatos, A. P. Air-Stable All-Inorganic Nanocrystal Solar Cells Processed from Solution. *Science* **2005**, *310*, 462−465.

(6) Beard, M. C.; Knutsen, K. P.; Yu, P.; Luther, J. M.; Song, Q.; Metzger, W. K.; Ellingson, R. J.; Nozik, A. J. Multiple Exciton Generation in Colloidal Silicon Nanocrystals. *Nano Lett.* **2007**, *7*, 2506−2512.

(7) Kamat, P. V. Quantum Dot Solar Cells. Semiconductor Nanocrystals as Light Harvesters. *J. Phys. Chem. C* **2008**, *112*, 18737−18753.

(8) Luther, J. M.; Law, M.; Beard, M. C.; Song, Q.; Reese, M. O.; Ellingson, R. J.; Nozik, A. J. Schottky Solar Cells Based on Colloidal Nanocrystal Films. *Nano Lett.* **2008**, *8*, 3488−3492.

(9) Johnston, K. W.; Pattantyus-Abraham, A. G.; Clifford, J. P.; Myrskog, S. H.; Hoogland, S.; Shukla, H.; Klem, E. J.; Levina, L.; Sargent, E. H. Efficient Schottky-quantum-dot photovoltaics: The roles of depletion, drift, and diffusion. *Appl. Phys. Lett.* **2008**, *92*, No. 122111.

(10) Leschkies, K. S.; Jacobs, A. G.; Norris, D. J.; Aydil, E. S. Nanowire-quantum-dot solar cells and the influence of nanowire length on the charge collection efficiency. *Appl. Phys. Lett.* **2009**, *95*, No. 193103.

(11) Pattantyus-Abraham, A. G.; Kramer, I. J.; Barkhouse, A. R.; Wang, X.; Konstantatos, G.; Debnath, R.; Levina, L.; Raabe, I.; Nazeeruddin, M. K.; Gratzel, M. Depleted-heterojunction colloidal quantum dot solar cells. *ACS Nano* **2010**, *4*, 3374−3380.

(12) Luther, J. M.; Gao, J.; Lloyd, M. T.; Semonin, O. E.; Beard, M. C.; Nozik, A. J. Stability assessment on a 3% bilayer PbS/ZnO quantum dot heterojunction solar cell. *Adv. Mater.* **2010**, *22*, 3704−3707.

(13) Gao, J.; Luther, J. M.; Semonin, O. E.; Ellingson, R. J.; Nozik, A. J.; Beard, M. C. Quantum Dot Size Dependent *J*−*V* Characteristics in Heterojunction ZnO/PbS Quantum Dot Solar Cells. *Nano Lett.* **2011**, *11*, 1002−1008.

(14) Ip, A. H.; Thon, S. M.; Hoogland, S.; Voznyy, O.; Zhitomirsky, D.; Debnath, R.; Levina, L.; Rollny, L. R.; Carey, G. H.; Fischer, A. Hybrid passivated colloidal quantum dot solids. *Nat. Nanotechnol.* **2012**, *7*, 577−582.

(15) Gonfa, B. A.; Zhao, H.; Li, J.; Qiu, J.; Saidani, M.; Zhang, S.; Izquierdo, R.; Wu, N.; El Khakani, M. A.; Ma, D. Air-processed depleted bulk heterojunction solar cells based on PbS/CdS core−shell quantum dots and TiO_2 nanorod arrays. *Sol. Energy Mater. Sol. Cells* **2014**, *124*, 67−74.

(16) Li, Y.; Wei, L.; Chen, X.; Zhang, R.; Sui, X.; Chen, Y.; Jiao, J.; Mei, L. Efficient PbS/CdS co-sensitized solar cells based on TiO_2 nanorod arrays. *Nanoscale Res. Lett.* **2013**, *8*, 1−7.

(17) Lan, X.; Bai, J.; Masala, S.; Thon, S. M.; Ren, Y.; Kramer, I. J.; Hoogland, S.; Simchi, A.; Koleilat, G. I.; Paz-Soldan, D. Self-Assembled, Nanowire Network Electrodes for Depleted Bulk Heterojunction Solar Cells. *Adv. Mater.* **2013**, *25*, 1769−1773.

(18) Lee, S.; Cho, I.-S.; Lee, J. H.; Kim, D. H.; Kim, D. W.; Kim, J. Y.; Shin, H.; Lee, J.-K.; Jung, H. S.; Park, N.-G. Two-step sol−gel method-based TiO_2 nanoparticles with uniform morphology and size for efficient photo-energy conversion devices. *Chem. Mater.* **2010**, *22*, 1958−1965.

(19) Kongkanand, A.; Tvrdy, K.; Takechi, K.; Kuno, M.; Kamat, P. V. Quantum Dot Solar Cells. Tuning Photoresponse through Size and Shape Control of CdSe-TiO_2 Architecture. *J. Am. Chem. Soc.* **2008**, *130*, 4007−4015.

DOI: 10.1021/acsami.5b00948
ACS Appl. Mater. Interfaces 2015, 7, 10324−10330

(20) Liu, B.; Khare, A.; Aydil, E. S. Synthesis of single-crystalline anatase nanorods and nanoflakes on transparent conducting substrates. *Chem. Commun. (Cambridge, U. K.)* **2012**, *48*, 8565−8567.
(21) Park, N. G.; van de Lagemaat, J.; Frank, A. J. Comparison of Dye-Sensitized Rutile- and Anatase-Based TiO_2 Solar Cells. *J. Phys. Chem. B* **2000**, *104*, 8989−8994.
(22) Liu, L.; Zhao, H.; Andino, J. M.; Li, Y. Photocatalytic CO_2 Reduction with H_2O on TiO_2 Nanocrystals: Comparison of Anatase, Rutile, and Brookite Polymorphs and Exploration of Surface Chemistry. *ACS Catal.* **2012**, *2*, 1817−1828.
(23) Luttrell, T.; Halpegamage, S.; Tao, J.; Kramer, A.; Sutter, E.; Batzill, M. Why is anatase a better photocatalyst than rutile?—Model studies on epitaxial TiO_2 films. *Sci. Rep.* **2014**, *4*, No. 4043.
(24) Kim, D. H.; Seong, W. M.; Park, I. J.; Yoo, E.-S.; Shin, S. S.; Kim, J. S.; Jung, H. S.; Lee, S.; Hong, K. S. Anatase TiO_2 nanorod-decoration for highly efficient photoenergy conversion. *Nanoscale* **2013**, *5*, 11725−11732.
(25) Kanie, K.; Sugimoto, T. Shape control of anatase TiO_2 nanoparticles by amino acids in a gel-sol system. *Chem. Commun. (Cambridge, U. K.)* **2004**, 1584−1585.
(26) Hines, M. A.; Scholes, G. D. Colloidal PbS nanocrystals with size-tunable near-infrared emission: observation of post-synthesis self-narrowing of the particle size distribution. *Adv. Mater.* **2003**, *15*, 1844−1849.
(27) Cho, I. S.; Chen, Z.; Forman, A. J.; Kim, D. R.; Rao, P. M.; Jaramillo, T. F.; Zheng, X. Branched TiO_2 Nanorods for Photoelectrochemical Hydrogen Production. *Nano Lett.* **2011**, *11*, 4978−4984.
(28) Moreels, I.; Lambert, K.; Smeets, D.; De Muynck, D.; Nollet, T.; Martins, J. C.; Vanhaecke, F.; Vantomme, A.; Delerue, C.; Allan, G. Size-dependent optical properties of colloidal PbS quantum dots. *ACS Nano* **2009**, *3*, 3023−3030.
(29) Tvrdy, K.; Kamat, P. V. Substrate Driven Photochemistry of CdSe Quantum Dot Films: Charge Injection and Irreversible Transformations on Oxide Surfaces. *J. Phys. Chem. A* **2009**, *113*, 3765−3772.
(30) Gaponenko, M. S.; Lutich, A. A.; Tolstik, N. A.; Onushchenko, A. A.; Malyarevich, A. M.; Petrov, E. P.; Yumashev, K. V. Temperature-dependent photoluminescence of PbS quantum dots in glass: Evidence of exciton state splitting and carrier trapping. *Phys. Rev. B* **2010**, *82*, No. 125320.
(31) Tang, J.; Brzozowski, L.; Barkhouse, D. A. R.; Wang, X.; Debnath, R.; Wolowiec, R.; Palmiano, E.; Levina, L.; Pattantyus-Abraham, A. G.; Jamakosmanovic, D. Quantum dot photovoltaics in the extreme quantum confinement regime: the surface-chemical origins of exceptional air-and light-stability. *ACS Nano* **2010**, *4*, 869−878.
(32) Bisquert, J.; Zaban, A.; Greenshtein, M.; Mora-Seró, I. Determination of rate constants for charge transfer and the distribution of semiconductor and electrolyte electronic energy levels in dye-sensitized solar cells by open-circuit photovoltage decay method. *J. Am. Chem. Soc.* **2004**, *126*, 13550−13559.
(33) Greene, L. E.; Law, M.; Yuhas, B. D.; Yang, P. ZnO-TiO_2 Core−Shell Nanorod/P3HT Solar Cells. *J. Phys. Chem. C* **2007**, *111*, 18451−18456.

DOI: 10.1021/acsami.5b00948
ACS Appl. Mater. Interfaces 2015, 7, 10324−10330